

TOWARD AN UNDERSTANDING OF THE RAPID DECLINE OF THE COSMIC STAR FORMATION RATE

ERIC F. BELL,¹ CASEY PAPOVICH,² CHRISTIAN WOLF,³ EMERIC LE FLOC'H,² JOHN A. R. CALDWELL,^{4,5} MARCO BARDEN,¹
EIICHI EGAMI,² DANIEL H. MCINTOSH,⁶ KLAUS MEISENHEIMER,¹ PABLO G. PÉREZ-GONZÁLEZ,²
G. H. RIEKE,² M. J. RIEKE,² JANE R. RIGBY,² AND HANS-WALTER RIX¹

Received 2004 August 23; accepted 2005 February 8

ABSTRACT

We present a first analysis of deep $24\ \mu\text{m}$ observations with the *Spitzer Space Telescope* of a sample of nearly 1500 galaxies in a thin redshift slice, $0.65 \leq z < 0.75$. We combine the infrared data with redshifts, rest-frame luminosities, and colors from COMBO-17 and with morphologies from *Hubble Space Telescope* images collected by the Galaxy Evolution from Morphology and SEDs (GEMS) and Great Observatories Origins Deep Survey (GOODS) projects. To characterize the decline in star formation rate (SFR) since $z \sim 0.7$, we estimate the total thermal IR luminosities, SFRs, and stellar masses for the galaxies in this sample. At $z \sim 0.7$, nearly 40% of intermediate- and high-mass galaxies (with stellar masses $\geq 2 \times 10^{10} M_{\odot}$) are undergoing a period of intense star formation above their past-averaged SFR. In contrast, less than 1% of equally massive galaxies in the local universe have similarly intense star formation activity. Morphologically undisturbed galaxies dominate the total infrared luminosity density and SFR density: at $z \sim 0.7$, more than half of the intensely star-forming galaxies have spiral morphologies, whereas less than $\sim 30\%$ are strongly interacting. Thus, a decline in major merger rate is not the underlying cause of the rapid decline in cosmic SFR since $z \sim 0.7$. Physical properties that do not strongly affect galaxy morphology—for example, gas consumption and weak interactions with small satellite galaxies—appear to be responsible.

Subject headings: galaxies: evolution — galaxies: fundamental parameters — galaxies: interactions — galaxies: starburst — galaxies: stellar content — infrared: galaxies

1. INTRODUCTION

It has become clear in the last decade that the average star formation rate (SFR) per unit comoving volume—the so-called cosmic SFR—has declined by an order of magnitude since $z \sim 1$ (Lilly et al. 1996; Madau et al. 1998; Hogg et al. 1998; Flores et al. 1999; Haarsma et al. 2000; Hopkins 2004). A number of physical processes may contribute to this decline, e.g., a declining rate of major galaxy mergers, a drop in the rate of minor tidal interactions, or the progressive consumption of cold gas. Yet, many empirical aspects of this declining cosmic SFR are frustratingly unclear. Does the star formation in disks evolve slowly, while merger-induced starbursts evolve rapidly? Does the decreasing number density of galaxies with high SFR reflect a decline in star formation in Milky Way–mass galaxies or reflect a disappearance of a population of bursting dwarf galaxies? In this paper, we present a first basic analysis of deep $24\ \mu\text{m}$ observations taken by the MIPS Team (Rieke et al. 2004; Papovich et al. 2004; Rigby et al. 2004). We combine these infrared (IR) data with the COMBO-17 redshift and spectral energy distribution (SED) survey (Wolf et al. 2004) and the largest existing *Hubble Space Telescope* (*HST*) Advanced Camera for Surveys (ACS) mosaic (the Galaxy Evolution from Morphology

and SEDs [GEMS]; Rix et al. 2004) to study nearly 1500 galaxies with $0.65 \leq z < 0.75$ in the $30' \times 30'$ extended Chandra Deep Field South (CDFs), with the goal of exploring the morphologies, stellar masses, and SFRs of galaxies and probing the physics driving the decrease in the cosmic SFR to the present day.

1.1. Understanding the Form of the Cosmic Star Formation History

The basic form of the cosmic star formation history (SFH) was initially established using observations of rest-frame ultraviolet (UV) luminosity (Lilly et al. 1996; Madau et al. 1996, 1998; Steidel et al. 1999), which in the absence of dust is an excellent indicator of the bolometric light output from young, massive stars. As rest-frame UV is redshifted into the optical, it becomes observationally straightforward to establish a deep census of unobscured young stars, well below the knee of the luminosity function. Yet, studies of both local and distant galaxies have shown that only a small fraction of the UV photons from $\sim L^*$ galaxies escape unhindered (dwarf galaxies are often optically thin to UV photons but do not significantly contribute to the SFR density; Wang & Heckman 1996; Adelberger & Steidel 2000; Bell 2003). Thus, the observed drop in UV luminosity density may not quantitatively track the drop in cosmic SFR.

Mindful of the limitations of rest-frame UV, other SFR indicators have been explored. Rest-frame optical line emission reflects the ionizing photon output from very massive young stars in the absence of dust extinction (see Kennicutt 1998 for a detailed discussion). Emission-line–derived SFRs have been studied intensively in the local universe (Gallego et al. 1995; Brinchmann et al. 2004) and have been probed out to $z \sim 3$ for the very brightest galaxies using rest-frame O II and Balmer line

¹ Max-Planck-Institut für Astronomie, Königstuhl 17, D-69117 Heidelberg, Germany; bell@mpia.de.

² Steward Observatory, University of Arizona, 933 North Cherry Avenue, Tucson, AZ 85721.

³ Department of Physics, Denys Wilkinson Building, University of Oxford, Keble Road, Oxford OX1 3RH, UK.

⁴ Space Telescope Science Institute, 3700 San Martin Drive, Baltimore, MD 21218.

⁵ Present address: University of Texas, McDonald Observatory, Fort Davis, TX 79734.

⁶ Department of Astronomy, University of Massachusetts, 710 North Pleasant Street, Amherst, MA 01003.

emission (Hogg et al. 1998; Yan et al. 1999; Glazebrook et al. 1999; Tresse et al. 2002; Hippelein et al. 2003; Erb et al. 2003). These studies find a considerable drop in the average SFR per unit volume in luminous galaxies since $z \sim 1$, but owing to the difficulty of measuring Balmer decrements of high-redshift galaxies, considerable uncertainties remain.

Radio and X-ray emission from distant galaxies also constrains their SFRs (Condon 1992; Cohen 2003). Observational constraints limit the applicability of both indicators to just the brightest sources at this stage; a substantial drop in the volume-averaged SFR in very luminous sources is again seen since $z \sim 1$ (e.g., Haarsma et al. 2000; Cohen 2003). Yet, both X-ray and radio luminosities are strongly boosted by the presence of an active galactic nucleus (AGN), and the physical origin of both is not well understood.

One of the most intuitive SFR indicators is the luminosity of a galaxy in the thermal IR. For most star-forming galaxies, the thermal IR emission is dominated by reprocessed UV photons from massive young stars that are dust enshrouded (see Kennicutt 1998 for an excellent review). For most galaxies the combined IR and UV luminosity is a relatively robust indicator of the bolometric output from young stars and therefore a good proxy for SFR (e.g., Gordon et al. 2000; Buat et al. 2002; Bell 2003), especially if the modest contribution to the IR flux from dust-reprocessed light from older stellar populations is accounted for (typically $\sim 30\%$ or less; Misiriotis et al. 2001; Bell 2003). Until recently, instrumental sensitivity has been a key limitation at these wavelengths; only galaxies with IR luminosities $\geq 10^{11} L_{\odot}$ have been observed at cosmologically interesting redshifts by the *Infrared Space Observatory (ISO)*. Through detailed modeling and analysis of these observations, it is clear that highly luminous IR galaxies were much more common at $z \sim 1$ than they are today (e.g., Flores et al. 1999; Elbaz et al. 2002; Mann et al. 2002; Pozzi et al. 2004). Observations of submillimeter emission from distant, intensely star-forming galaxies have extended this picture to $z \geq 2$ (e.g., Blain et al. 1999). Yet, despite this encouraging progress, it is still unclear how the evolution of these highly luminous galaxies is linked to the much more numerous fainter galaxies that dominate the volume-averaged SFR.

1.2. Understanding the Physical Drivers of Star Formation

A wide range of processes may contribute to the order-of-magnitude drop in cosmic SFR since $z \sim 1$: major mergers, tidal interactions, gas consumption, ram pressure stripping, galaxy harassment, or the secular evolution of bars. Deciding which processes dominate involves a number of observational and interpretive challenges. As an example, it is challenging to measure the major merger rate robustly; close-pair statistics suffer from contamination, automated asymmetry measures are sensitive to contamination from irregular galaxies and very close projected pairs, and visual morphological classifications are subjective, and less sensitive to prograde interactions owing to their lack of pronounced tidal tails.

There is evidence that these different physical processes play a role in shaping the SFRs of galaxies. Many merging galaxies form stars intensely (e.g., Sanders & Mirabel 1996). Given the observational evidence for a drop in the merger rate since $z \sim 1$ (e.g., Le Fèvre et al. 2000; Patton et al. 2002; Conselice et al. 2003), it is indeed plausible that the decline in the volume-averaged cosmic SFR is driven at least in part by this drop in merger rate. Furthermore, minor interactions seem to enhance SFRs, at least in the local universe (e.g., Barton et al. 2000), plausibly by exciting unstable modes such as bars or strong

transient spiral arms in the affected galaxies. The exhaustion of cold gas could also play a role. Indeed, most massive nearby galaxies have low gas fractions $\lesssim 10\%$ (e.g., Kennicutt et al. 1994; Bell & de Jong 2000), and the current SFRs of many local galaxies will exhaust the available gas supply in ~ 5 Gyr (e.g., Kennicutt et al. 1994). It is possible that fresh infall or recycled gas can help to sustain star formation for a longer time. Yet, it is also possible that we live in a special epoch, when the star formation in massive galaxies is switching off.

1.3. The Object of This Paper

This paper is one of a series in which we explore different aspects of the declining cosmic SFR. Wolf et al. (2005) study the contribution of different galaxy morphologies to the rest-frame 2800 Å luminosity density for rest-frame *B*-band-selected galaxies in a thin $0.65 \leq z < 0.75$ redshift slice from COMBO-17 and GEMS. In this paper, we supplement this optically selected sample with 24 μm data from *Spitzer* to explore the contribution of obscured star formation.⁷ Le Flocc'h et al. (2005) explore the IR luminosity function over the range $0 < z < 1$ using MIPS 24 μm data and COMBO-17 redshifts. C. Papovich et al. (2005, in preparation) explore the morphologies of the galaxies that dominate the turnover in the 24 μm number counts, as a clue to understanding the drivers of IR-obscured star formation.

In this paper, we study the MIPS 24 μm properties of a complete sample of rest-frame *B*-band-selected $0.65 \leq z < 0.75$ galaxies in the CDFS.⁸ Owing to the high sensitivity and relatively tight point-spread function (PSF) of 24 μm *Spitzer* observations, many more star-forming galaxies are detected at 24 μm than at 70 and 160 μm . We use IR template spectra, tuned to reproduce the whole range of local galaxy IR SEDs, to transform 24 μm luminosity into total IR luminosity. For the smaller area imaged by *Chandra* to date, we incorporate the *Chandra* X-ray data (Alexander et al. 2003) to explore the importance of AGNs at 24 μm (see also Rigby et al. 2004). Our main goals are to identify all $z \sim 0.7$ galaxies with high SFRs, explore their morphologies, and characterize the importance of massive starbursting galaxies compared to the present-day universe, as a probe of the physics driving the declining cosmic SFR.

The paper is set out as follows. In § 2 we discuss the data. In § 3 we outline the methods used to estimate total IR flux, SFR and stellar mass, and the main sources of uncertainty. In § 4 we present trends in the IR/UV ratio. In § 5 we explore the contribution of different morphological types to the total SFR at $z \sim 0.7$. In § 6 we discuss intense star formation in massive galaxies and how this changes over the last 7 Gyr. In § 7 we compare with existing data, explore the contribution of AGNs, compare with theory, and discuss future improvements in this analysis. In § 8 we present our conclusions. Appendices A and B discuss possible incompleteness in our optically selected catalog and uncertainties in the galaxy morphological classifications. Throughout, we express the estimated integrated UV and IR luminosities in terms of the bolometric luminosity of the

⁷ An additional advantage of adopting such a narrow redshift slice for this paper is that the effects of *differential* $(1+z)^4$ surface brightness dimming, morphological *k*-corrections, and uncertainties in the conversion of 24 μm flux to total IR are minimized.

⁸ At this stage, we cannot and do not study completely obscured galaxies with extremely faint or nonexistent UV/optical detections. Preliminary indications are that these optically faint IR sources are optically faint largely owing to their relatively high redshift ($z \geq 1$; e.g., Papovich et al. 2004) rather than having a lower redshift and higher obscuration. See Appendix A, where this issue is explored in more detail.

Sun $L_{\odot} = 3.9 \times 10^{26}$ W. We assume $\Omega_m = 0.3$, $\Omega_{\Lambda} = 0.7$, and $H_0 = 70 \text{ km s}^{-1} \text{ Mpc}^{-1}$ (Spergel et al. 2003). Estimates of SFR and stellar mass assume a universally applicable Kroupa (2001) initial mass function (IMF).⁹

2. THE DATA

2.1. MIPS Data

Spitzer observed a $1^{\circ} \times 0.5^{\circ}$ field around the CDFS in 2004 January and February as part of the time allocated to the *Spitzer* Guaranteed Time Observers (GTOs). The MIPS 24 μm data were taken in slow scan–map mode, with individual exposures of 10 s. We reduced the individual image frames using a custom data analysis tool (DAT) developed by the GTOs (Gordon et al. 2005).¹⁰ The reduced images were corrected for geometric distortion and combined to form full mosaics. The final mosaic has a pixel scale of $1''.25 \text{ pixel}^{-1}$ and an image PSF FWHM of $\sim 6''$. The *Spitzer* astrometry is aligned to the ESO Imaging Survey (Arnouts et al. 2001) with a typical accuracy $\sim 0''.5$. The overall astrometric solution is then shifted by nearly $1''$ by matching to the much sparser Two Micron All Sky Survey catalog (2MASS). This revised astrometric solution is matched to $\leq 0''.1$ with the COMBO-17 coordinate system.

Source detection and photometry were performed using techniques described in Papovich et al. (2004); based on the analysis in that work, we estimate that our source detection is 80% complete at 83 μJy in the 24 μm image. Based on our noise estimates, the photon noise in the 24 μm image is roughly equal to the confusion noise at this depth (see, e.g., Dole et al. 2004).

2.2. Optical Data: COMBO-17 and GEMS

To date, COMBO-17 has surveyed three disjoint $\sim 34' \times 33'$ southern and equatorial fields to deep limits in five broad and 12 medium passbands. Using these deep data in conjunction with nonevolving galaxy, star, and AGN template spectra, objects are classified and redshifts assigned for $\sim 99\%$ of the objects to a limit of $m_R \sim 23.5$. Typical galaxy redshift accuracy is $\delta z/(1+z) \sim 0.02$ (Wolf et al. 2004), allowing construction of ~ 0.1 mag accurate rest-frame colors and absolute magnitudes (accounting for distance and k -correction uncertainties). Astrometric accuracy is $\sim 0''.1$.

To explore galaxy morphology in the rest-frame optical from a single observed passband, we study galaxies in one thin redshift slice. Here we select galaxies from COMBO-17 in the CDFS for morphological classification in the narrow interval $0.65 \leq z < 0.75$ (corresponding to $\Delta t \sim 0.5$ Gyr, minimizing galaxy evolution across this slice). At this redshift, F850LP samples roughly rest-frame V band, and *Spitzer*'s 24 μm passband samples rest-frame 14 μm , allowing comparison with local samples. Furthermore, $z \sim 0.7$ is close to the median redshift of COMBO-17, maximizing the sample size.

We use F850LP imaging from the GEMS survey (Rix et al. 2004) to provide $0''.07$ resolution rest-frame V -band data for 1492 galaxies with $0.65 \leq z < 0.75$. GEMS surveys a $\sim 28' \times 28'$ portion of the CDFS in the F606W and F850LP passbands to deep limits using the ACS (Ford et al. 2003) on *HST*. The GEMS area is covered by a multiple, overlapping image mosaic

that includes the smaller but deeper Great Observatories Origins Deep Survey (GOODS) area (Giavalisco et al. 2004). One orbit per pointing was spent on each passband (63 GEMS tiles and 15 GOODS tiles), allowing galaxy detection to a limiting surface brightness within the half-light radius of $\mu_{\text{F850LP, AB}} \sim 24 \text{ mag arcsec}^{-2}$ (Rix et al. 2004). At $z = 0.7$, ACS resolution corresponds to ~ 500 pc resolution, roughly equivalent to $\sim 1''$ resolution at Coma Cluster distances.

Galaxy classification was carried out by eye on the $z \sim 0.7$ sample by E. F. B., C. W., and D. H. M. using the GEMS F850LP imaging.¹¹ In what follows, we adopt by-eye classification bins of E/S0, Sa–Sd, irregular/compact (Irr), and peculiar/clearly interacting (Pec/Int). Galaxies were classified on the basis of both central light concentration and smoothness. E/S0 galaxies were required to have dominant spheroids and smooth light distributions. Sa–Sd galaxies were required to have prominent disks with signs of ongoing star formation. Galaxies classified as irregular are chosen to be similar in morphology to low surface brightness and Magellanic irregular galaxies in the local universe; their irregular light distributions appear to the eye to result from stochastic variations and bursts in their SFH rather than from any interaction. In contrast, the peculiar/clearly interacting designation requires that galaxies have signs of tidal features and/or multiple nuclei, with morphologies suggestive of a major galaxy merger or merger remnant.¹² These classifications are discussed in detail and examples of each class are shown in Wolf et al. (2005).

Obviously, these classifications are subjective and depend on the depth of the imaging material. In particular, comparison with deeper GOODS data for a subset of 290 galaxies in this redshift slice has shown that the fraction of faint clearly interacting galaxies in GEMS is slightly underestimated (Wolf et al. 2005). While the ideal solution would be to simply consider only the GOODS data, number statistics is a key limitation: there are ~ 80 galaxies at $z \sim 0.7$ in the GOODS area that are detected at 24 μm , compared to the ≥ 400 galaxies detected in the whole GEMS area. We therefore choose to study galaxies from the whole GEMS area, adjusting the GEMS-only classifications as a function of IR luminosity to account for the underestimated faint interaction fraction. We address this topic and the scatter among the three different classifiers where relevant in § 5 and Appendix B.

2.3. Cross-Correlation of the IR and Optical Data

At this stage, we have simply correlated the 24 μm imaging catalog with the COMBO-17 catalog. The 24 μm footprint does not exactly match that of COMBO-17; of the 1727 COMBO-17 galaxies in our redshift slice, 1436 are covered by the 24 μm data. A subsample of 1306 of these are covered by the GEMS mosaic and have full morphological, 24 μm , and redshift information. Sources are matched within $2''$. Roughly 96% of 24 μm sources have only one match in the COMBO-17 catalog. The other 4% have two matches in the COMBO-17 catalog; the

⁹ In the case where the stellar IMF varies as a function of time and/or from galaxy to galaxy, neither SFRs nor stellar masses will be robust except perhaps at the order-of-magnitude level.

¹⁰ To date, our preliminary tests indicate that the DAT reduction of MIPS 24 μm data is nearly identical to that provided by the *Spitzer* Science Center pipeline.

¹¹ Automated classification using profile fitting is highly consistent with the by-eye classifications that we adopt here, in terms of differentiating between bulge-dominated galaxies and disk-dominated galaxies (Bell et al. 2004). Work on automated diagnostics of galaxy interactions in GEMS is ongoing and will be discussed in a future work.

¹² In many works galaxies that do not fit onto the Hubble sequence are labeled irregular, where no attempt is made to characterize the driver of the irregularities. Because we wish to gain insight into the role of interactions in driving the star formation activity of galaxies, we attempt, perhaps naively, to distinguish between galaxies with clear signs of interaction (Pec/Int) and those without (Irr).

closest positional match is taken in these cases.¹³ A 24 μm catalog constructed using optical positions as prior constraints would address many of these limitations but is challenging to implement at this stage; we defer a complete analysis of this type to a later date. In total, 442 galaxies with $0.65 \leq z < 0.75$ are detected at 24 μm and have a match in COMBO-17 (397 overlap with GEMS); the rest of the COMBO-17 sources without 24 μm detections are assigned 5σ upper limits of 83 μJy .¹⁴ In Appendix A we explore the possibility that our sample selection may be biased against highly obscured IR-luminous galaxies. We find that $z \sim 0.7$ IR-luminous galaxies should be bright enough to be detected and successfully classified by COMBO-17, suggesting that the sample selection and main conclusions of this paper should be robust to this potential source of incompleteness.

3. ANALYSIS

3.1. Estimating Total IR Luminosity

Local IR-luminous galaxies show a tight correlation between rest-frame 12–15 μm luminosity and total IR luminosity (e.g., Spinoglio et al. 1995; Chary & Elbaz 2001; Roussel et al. 2001; Papovich & Bell 2002), with a scatter of ~ 0.15 dex. Following Papovich & Bell (2002), we use this correlation to construct total IR luminosity from the observed-frame 24 μm data (corresponding to rest-frame $\sim 14 \mu\text{m}$). We use the full range of Dale et al. (2001) model template spectra to calculate the conversion from observed-frame 24 μm to 8–1000 μm total IR luminosity,¹⁵ we adopt the mean value as our estimate of IR luminosity and the rms as our estimate of conversion uncertainty. The mean correction factor corresponds approximately to $L_{\text{IR}} \sim 10\nu l_\nu(24 \mu\text{m})$ to within 20%, where $l_\nu(24 \mu\text{m})$ is the monochromatic luminosity at observed-frame 24 μm ; the template scatter around this mean is larger, ~ 0.3 dex. Different choices of template (e.g., Devriendt et al. 1999) or the adoption of a luminosity-dependent conversion yield similar results. The 5σ detection limit of 83 μJy corresponds to a limiting IR luminosity of $6 \times 10^{10} L_\odot$, or $\sim 6 M_\odot \text{ yr}^{-1}$ in terms of an IR-derived SFR.

The conversion from the 24 μm photometry to 8–1000 μm IR luminosity should be accurate to within a factor of 2 or better, which is adequate for our purposes. There are two types of error. First, the conversion depends on fitting templates to the galaxy SEDs. There is a total range of a factor of 2 difference between the conversions that would be predicted by various templates for galaxies in the appropriate luminosity range of $\sim 10^{11} L_\odot$ (Devriendt et al. 1999; Dale et al. 2001; Chary & Elbaz 2001; Lagache et al. 2003, 2004). Second, there is a possibility that the infrared properties of typical high-luminosity galaxies differ at $z \sim 0.7$ from those of the local galaxies used in developing the templates. The evidence available to us now suggests that the IR SEDs of $z \gtrsim 0.7$ seem to be adequately spanned by the IR SEDs of local galaxies: the evolution of the mid-IR–radio correlation to $z \sim 1$ (e.g., Elbaz et al. 2002; Appleton et al. 2004), 15–24 μm flux ratios from *ISO* and *Spitzer* for galaxies at $z \sim 1$ (Elbaz et al. 2005), and mid-IR spectra from *Spitzer* of $z \sim 1$ ultraluminous infrared galaxies

(ULIRGs; L. Yan 2004, private communication). This issue will be significantly clarified by future work from *Spitzer* and *Herschel*.

3.2. Estimating Star Formation Rates

We estimate SFRs using the combined UV and IR emission of the sample galaxies. This SFR estimator accounts for both direct light from young stars from the UV and obscured light from the IR, giving a complete census of the bolometric luminosity of young stars in the galaxy (e.g., Gordon et al. 2000). The primary difficulties affecting this SFR estimator are (1) the poorly constrained fraction of IR light from dust heated by old stars and (2) geometry, in the sense that the IR light is radiated isotropically, whereas the UV light escapes along preferred directions (such as out of the plane of a disk galaxy). Future works will be able to address point 1 through more detailed modeling of UV/optical/IR SEDs and will be able to ascertain to what extent averaging over inclination angles effectively addresses point 2.

In practice, we estimate the SFR ψ using a calibration derived from the PEGASE stellar population models (see Fioc & Rocca-Volmerange 1997 for a description of an earlier version of the model), assuming a 100 Myr old stellar population with constant SFR and a Kroupa (2001) IMF:

$$\frac{\psi}{M_\odot \text{ yr}^{-1}} = 9.8 \times 10^{-11} (L_{\text{IR}} + 2.2L_{\text{UV}}), \quad (1)$$

where L_{IR} is the total IR luminosity and $L_{\text{UV}} = 1.5\nu l_{\nu,2800}$ is a rough estimate of the total integrated 1216–3000 \AA UV luminosity, derived using the 2800 \AA rest-frame luminosity $l_{\nu,2800}$ from COMBO-17. The factor of 1.5 in the 2800 \AA -to-total UV conversion accounts for the UV spectral shape of a 100 Myr old population with constant SFR. The SFR is derived assuming that L_{IR} reflects the bolometric luminosity of young, completely obscured populations and that L_{UV} reflects the contribution of unobscured stars, which must be multiplied by a factor of 2.2 to account for light emitted longward of 3000 \AA and shortward of 1216 \AA by the unobscured young stars. In practice, the SFRs are dominated by the IR contribution for the range of SFRs explored in this paper. This SFR calibration is derived under identical assumptions as the UV and IR SFR calibrations presented by Kennicutt (1998). Our SFR calibration is consistent with Kennicutt (1998) to better than 30% once different IMFs are accounted for. Bell (2003) tested UV+IR-derived SFRs against carefully extinction-corrected $\text{H}\alpha$ and radio-derived SFRs for a large sample of local star-forming galaxies, finding excellent agreement with 0.3 dex scatter and no offset. Accordingly, we adopt a systematic error estimate of 0.3 dex (dominated by 24 μm -to-total conversion error) and 0.4 dex random error (with contributions from both 24 μm -to-total conversion and limitations in UV+IR-derived SFRs). These error estimates are supported by comparisons between *ISO* 15 μm -derived SFRs with carefully constructed Balmer line SFRs for galaxies at $0 < z < 0.8$: there was no offset between the SFR scales and 0.4 dex random scatter for SFRs less than $250 M_\odot \text{ yr}^{-1}$ (Flores et al. 2004).

3.3. Estimating Stellar Mass

To understand how the instantaneous SFR in a galaxy compares with its mean past rate, it is necessary to estimate the existing stellar mass. Under the assumption of a universally applicable stellar IMF, there is a tight correlation between rest-frame optical color and stellar M/L , which is rather insensitive

¹³ This effect may lead to 1%–2% incompleteness if two sources with 24 μm emission are mistakenly blended into one source.

¹⁴ Sources near the map edges where the noise is nonuniform have been disregarded in this work.

¹⁵ Total 8–1000 μm IR luminosities are ~ 0.3 dex higher than the 42.5–122.5 μm luminosities defined by Helou et al. (1988), with an obvious dust temperature dependence.

to details of galaxy SFH, dust content, and metallicity (e.g., Bell & de Jong 2001; Bell et al. 2003; Kauffmann et al. 2003). On the basis of this correlation, we estimate stellar mass M_* using the rest-frame B - and V -band magnitudes:

$$\log_{10} \frac{M_*}{M_\odot} = -0.4(V - 4.82) + [-0.628 + 1.305(B - V) - 0.15], \quad (2)$$

where the -0.15 dex term converts the stellar masses to a Kroupa (2001) IMF.¹⁶ Systematic and random errors in stellar masses are roughly 0.3 dex, owing primarily to the effects of dust, galaxy age, and bursts of star formation (Bell & de Jong 2001; Bell et al. 2003; Franceschini et al. 2003). For stellar populations completely dominated by ≤ 1 Gyr old stars, the luminosity at a given color is roughly a factor of 3 higher than for galaxies with a wider range of stellar ages. Because equation (2) assumes a wide range in stellar age, the stellar masses of galaxies with recent very large bursts of star formation will be *overestimated*.

4. TRENDS IN IR-TO-UV RATIO WITH SFR

The comparison of UV and IR luminosities shows that, both on a galaxy-to-galaxy basis and globally, the SFR estimates discussed below are essentially IR derived, with a minor $\leq 30\%$ contribution from the UV. To assess the relative importance of UV and IR light in individual galaxies at $z \sim 0.7$, Figure 1 shows IR/UV as a function of SFR, as derived from the IR and UV luminosities using equation (1). The range of IR/UV and the trend with total luminosity in the $z \sim 0.7$ sample is very similar to that observed in the local universe (e.g., Wang & Heckman 1996; Adelberger & Steidel 2000; Bell 2003), indicating little or no evolution in the relative proportion of obscured star formation at least to $z \sim 0.7$.¹⁷ This is illustrated in Figure 1, where the locus of local star-forming galaxies is also shown.¹⁸ Galaxies with SFRs $\geq 6 M_\odot \text{ yr}^{-1}$ have $\text{IR}/\text{UV} \geq 10$, indicating that uncorrected UV SFRs are gross underestimates of the true SFR for the most intensely star-forming systems.

The cumulated total IR luminosity of all detected sources in this redshift slice is $(7 \pm 3) \times 10^{13} L_\odot$, where the error bar is dominated by our assumed error in $24 \mu\text{m}$ to total IR conversion.¹⁹ If we assign detections at $83 \mu\text{Jy}$ to all the upper limits, we derive an upper limit to the total IR luminosity of twice the value from the detected galaxies. This result agrees with the number counts and our current IR luminosity function estimates, which indicate that about $\frac{2}{3}$ of the total background at $24 \mu\text{m}$ is resolved at our detection limit (Papovich et al. 2004; Le Flocc'h et al. 2005). We conclude that the total IR luminosity

¹⁶ More sophisticated stellar mass estimates, based on direct modeling of COMBO-17's observed 17-passband SED (A. Borch et al. 2005, in preparation), agree with these color-based estimates with no systematic offset and $\leq 40\%$ random scatter.

¹⁷ This is also consistent with a sample of very luminous IR-luminous $z \sim 1$ starbursts from a $15 \mu\text{m}$ -selected *ISO* sample (Aussel et al. 1999, as discussed by Adelberger & Steidel).

¹⁸ This has been adapted from their Fig. 11a, where $\log_{10} \text{SFR} \sim \log_{10}(L_{1600} + L_{\text{bol,dust}}) - 9.7$, accounting for our adoption of $H_0 = 70 \text{ km s}^{-1} \text{ Mpc}^{-1}$. The UV luminosity is estimated by $L_{\text{UV}} \sim \nu f_{\nu,1600}$ (derived using PEGASE for a 100 Myr old stellar population with constant SFR; coincidentally, the UV spectral shape cancels out, leaving 1216–3000 Å luminosity equal to monochromatic 1600 Å luminosity). These estimates of SFR and IR/UV should be consistent with our estimates, to within the considerable systematic uncertainties.

¹⁹ This is the total luminosity in the volume-limited $0.65 \leq z < 0.75$ sample and so is in essence a luminosity density. We choose to express quantities in terms of total luminosities at this time owing to concerns about cosmic variance. This topic is considered in more detail by Le Flocc'h et al. (2005).

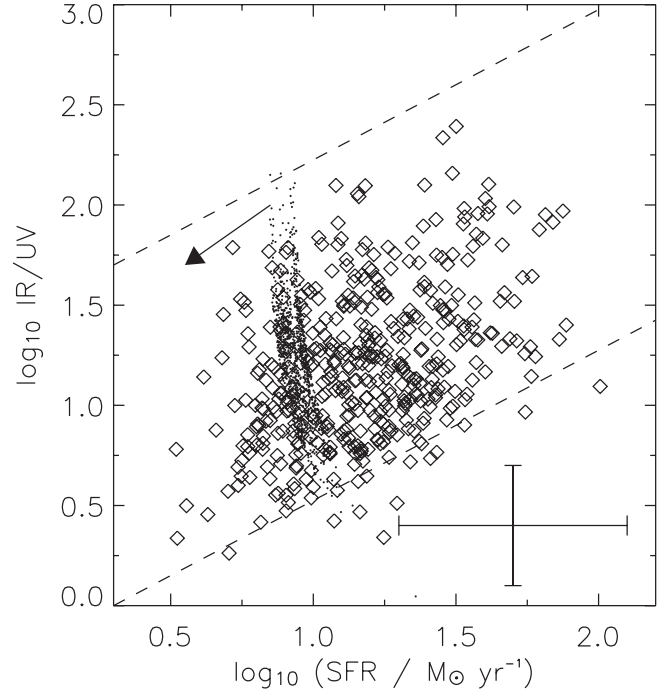


FIG. 1.—IR/UV as a function of SFR. Diamonds show galaxies detected with MIPS at $24 \mu\text{m}$, whereas points show $24 \mu\text{m}$ upper limits for galaxies not detected by MIPS; these limits will move toward the lower left with a slope of unity as shown by the arrow and therefore are consistent with the trend observed for the detected galaxies. The dashed lines outline the local relation as derived by Adelberger & Steidel (2000). The error bars show our uncertainty estimates: 0.3 dex in IR/UV (dominated by $24 \mu\text{m}$ -to-total conversion uncertainty) and a 0.4 dex SFR uncertainty.

in this redshift slice is $\sim 10^{14} L_\odot$. In comparison, the total UV luminosity in this redshift slice is $(1.5 \pm 0.3) \times 10^{13} L_\odot$ when the luminosity function is extrapolated to zero luminosity (using the 2800 \AA luminosity function determined for this redshift slice by Wolf et al. 2005).²⁰ Thus, at $z \sim 0.7$, the ratio of IR to UV luminosity density is $\sim 7_{-3}^{+4}$.

5. EXPLORING THE RELATIONSHIP BETWEEN STAR FORMATION RATE AND MORPHOLOGY

In this section, we explore which types of galaxies account for the bulk of star formation in the $z \sim 0.7$ universe, when the universe was only half its present age.

5.1. The Relationship between Optical Properties and Star Formation

In Figure 2, we show the rest-frame optical $U - V$ color and V -band absolute magnitude of all galaxies in the $0.65 \leq z < 0.75$ slice, split by visual morphological type. Filled symbols denote galaxies detected at $24 \mu\text{m}$, while open symbols denote galaxies for which only $24 \mu\text{m}$ upper limits ($83 \mu\text{Jy}$) were available. In both cases, symbol size scales with the logarithm of SFR or its upper limit.

Among visually classified E/S0 galaxies, those that are blue in the optical are also clearly detected at $24 \mu\text{m}$. Ignoring for the moment active nuclei (see § 7), we attribute this $24 \mu\text{m}$ flux to

²⁰ It is worth noting that there is a difference in how we define luminosity densities compared with Wolf et al. (2003, 2005). These papers express luminosity densities in terms of monochromatic solar luminosities at a given rest-frame wavelength, whereas we choose to present L_{UV} in terms of bolometric solar luminosities.

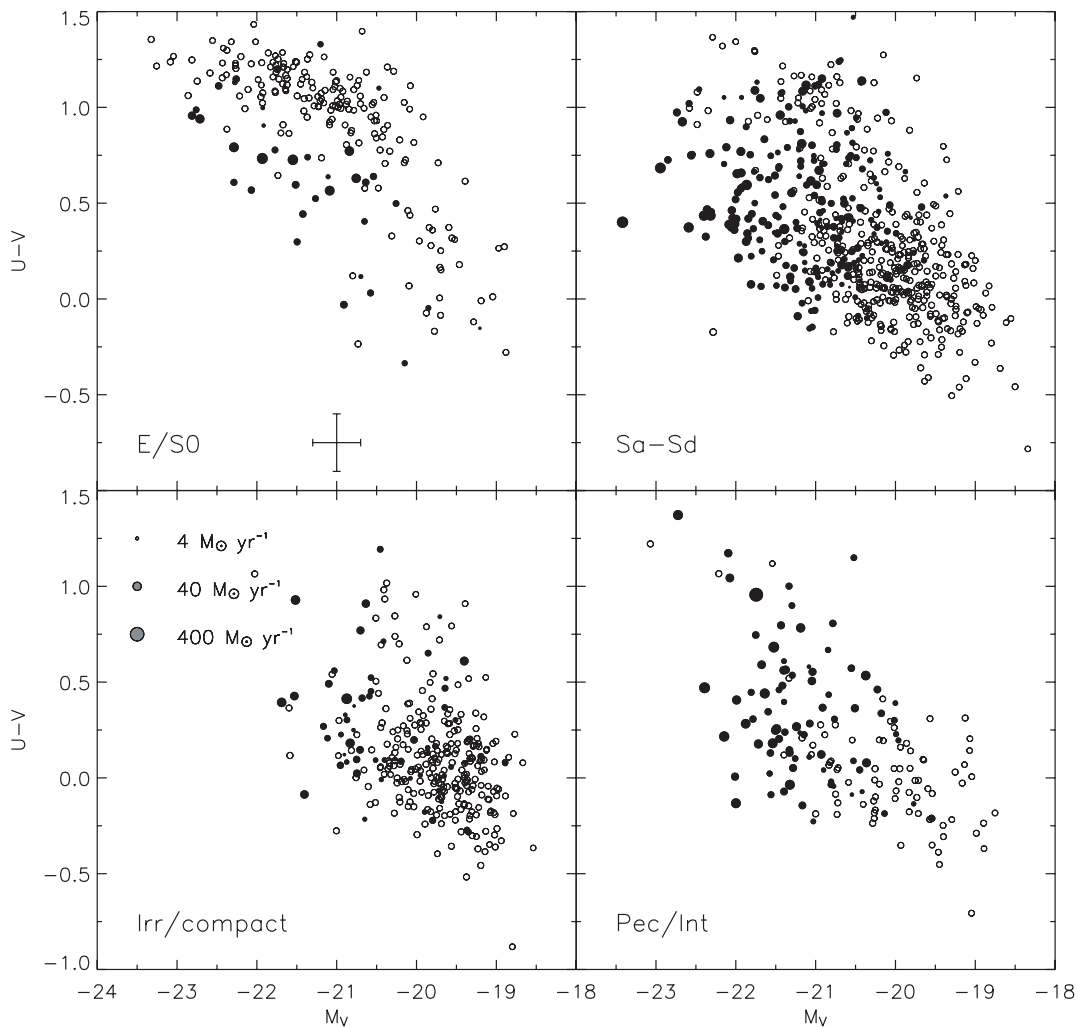


FIG. 2.—Rest-frame $U - V$ color of 1436 optically selected $0.65 \leq z < 0.75$ galaxies from COMBO-17/GEMS as a function of visually classified rest-frame V -band galaxy morphology (classifications are adopted at random from three classifiers). Symbol size scales with the logarithm of the estimated SFR: filled circles denote galaxies with MIPS $24 \mu\text{m}$ detections (therefore the symbol size denotes SFR estimated using IR+UV), whereas the open circles show upper limits on the SFR, derived using the observed UV luminosity and the upper limits on $24 \mu\text{m}$ flux.

rapid star formation. In contrast, there are very few galaxies on the red sequence with $24 \mu\text{m}$ detections. Thus, red E/S0 galaxies are IR-faint, which suggests that their red optical colors are the result of dominant old stellar populations, not dust-obscured star formation.

Blue visually classified spiral galaxies (Sa–Sd) are frequently detected in the IR. Many optically red spiral galaxies are IR-faint and are thus red because of their ancient stellar populations. Yet, a rather higher fraction of red spirals are detected at $24 \mu\text{m}$ compared to red E/S0 galaxies, especially at fainter optical luminosities, indicating a more important role for dust-reddened spiral galaxies. Morphologically classified irregular galaxies are typically somewhat less luminous, and owing to their lower SFRs are less frequently detected by MIPS; however, they are qualitatively similar to low-luminosity spirals.

The vast majority of visually classified peculiar and clearly interacting galaxies are detected at $24 \mu\text{m}$; indeed, the few non-detections are almost all relatively faint and are not expected to be detected at $24 \mu\text{m}$ for plausible UV/IR ratios. Interestingly, most red Pec/Int galaxies are strong $24 \mu\text{m}$ sources (including the brightest galaxy at $24 \mu\text{m}$ in the $0.65 \leq z < 0.75$ slice, which is an interacting galaxy on the blue edge of the red sequence). Therefore, we conclude that (1) almost all of our vi-

sually classified Int/Pec galaxies are intensely star-forming at the epoch of observation and (2) the optical colors of Int/Pec galaxies largely reflect their dust content, rather than their SFH.

In summary, the optical color of morphologically undisturbed galaxies (E/S0 and Sa–Sd galaxies) reflects SFH in a broad sense: most red early-type galaxies and a significant fraction of red spiral galaxies are non–star-forming, whereas the blue early- and late-type galaxies have important amounts of current star formation as probed by the IR. In contrast, clearly interacting and peculiar galaxies have strong IR-luminous star formation irrespective of their optical properties (as is expected of very dusty star-forming systems).

5.2. The Contribution of Different Galaxy Types to the Cosmic SFR

An important question is the relative contribution of galaxies with different morphological types to the total SFR density at $z \sim 0.7$. The cosmic-averaged SFR has dropped by a factor of 3 since $z \sim 0.7$ as measured in the IR (e.g., Flores et al. 1999; Pozzi et al. 2004), radio (e.g., Haarsma et al. 2000), $\text{H}\alpha$ (e.g., Tresse et al. 2002; Pérez-González et al. 2003), or UV (e.g., Lilly et al. 1996; Schiminovich et al. 2005). Thus, an understanding of the relative contribution of different galaxy types to

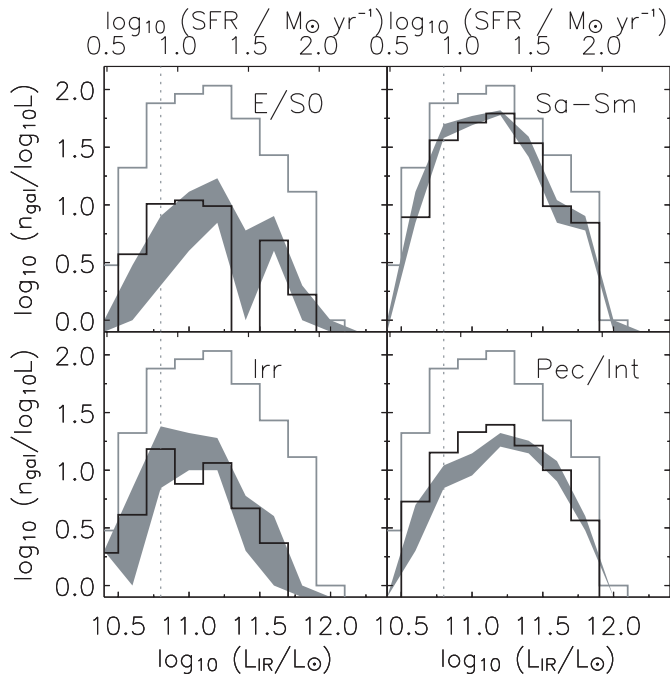


FIG. 3.—Estimated 8–1000 μm luminosity function, split by morphological type for 397 galaxies at $0.65 \leq z < 0.75$. Only galaxies detected at $24 \mu\text{m}$ are shown, and no attempt to extrapolate to lower IR luminosities has been made; the sample is grossly incomplete below $\sim 6 \times 10^{10} L_{\odot}$ as denoted by the gray dotted line. In each panel, the gray solid histogram shows the total IR luminosity function. The shaded area shows the IR luminosity function split by galaxy type using GEMS-derived galaxy classifications, where the extent of the shaded area explicitly shows the differences in IR luminosity function given by the three different classifiers. The black histogram shows the IR luminosity function, averaged over the three different classifiers and corrected to reproduce the increased fraction of clearly interacting galaxies seen in GOODS-depth data, as described in Appendix B.

the cosmic SFR at $z \sim 0.7$ will constrain the types of galaxy that need to “switch off” their star formation activity between $z \sim 0.7$ and the present day, giving insight into the physical mechanisms driving this evolution.

In Figure 3, we show the distribution of estimated IR luminosity as a function of galaxy type for $24 \mu\text{m}$ –detected galaxies at $z \sim 0.7$; the top axes show the equivalent SFRs. We choose not to normalize the luminosity function to the observed volume at this stage owing to concerns about cosmic variance (e.g., Somerville et al. 2004); a thorough analysis of evolution in the IR luminosity function is presented in a companion paper by Le Flocc’h et al. (2005). We do not extrapolate the IR luminosity function below the $24 \mu\text{m}$ detection limit at $\sim 6 \times 10^{10} L_{\odot}$.

The IR luminosity density for $10.7 \lesssim \log_{10}(L_{\text{IR}}/L_{\odot}) \lesssim 11.5$ is dominated by spiral galaxies, with an important contribution from clearly interacting galaxies. Morphologically classified E/S0 galaxies and irregulars contribute, but they play lesser roles. Clearly interacting galaxies make an increasingly important contribution at $\log_{10}(L_{\text{IR}}/L_{\odot}) \gtrsim 11.3$. This behavior resembles that in the local universe, where almost all galaxies with $\log_{10}(L_{\text{IR}}/L_{\odot}) \gtrsim 11.8$ show clear signs of interaction (Sanders & Mirabel 1996). Integrating over the whole distribution of galaxies detected at $24 \mu\text{m}$, we find that the fractional contributions of spiral, E/S0, Pec/Int, and irregular galaxies to the total integrated IR luminosity density are 0.51:0.10:0.28:0.11.

To probe the uncertainties in the relative contributions to the SFR density from different galaxy types, we explore two limiting cases: (1) all $24 \mu\text{m}$ nondetections have no IR flux (i.e., their SFR is measured purely from the UV); or (2) all $24 \mu\text{m}$ non-

detections emit at the detection upper limit at this wavelength of $83 \mu\text{Jy}$. In the first case, the split of SFR is (spiral:E/S0:Pec/Int:Irr) 0.51:0.10:0.26:0.13, very similar to the split in terms of observed IR flux (because the UV is a relatively small contribution to the total SFR density). In the second case, where limits are all taken to be marginal detections, the split is 0.47:0.15:0.18:0.20. Because of the preponderance of E/S0 and Irr nondetections, the relative importance of these classes is increased (arguably, rather artificially). In neither of these cases are the contributions from optically faint galaxies (i.e., those galaxies fainter than $M_V \gtrsim -19$) accounted for. Because the integral over a luminosity function is dominated by $\sim L^*$ galaxies, our limitation to relatively bright sources does not prevent us from qualitatively constraining the contribution of different galaxy types. Nonetheless, it is clear that the detailed form of the distribution of SFRs to lower limits will importantly affect the quantitative contributions of the different galaxy types and is arguably the largest source of systematic uncertainty in this paper.

To summarize, the SFR density at $z \sim 0.7$ is dominated by morphologically normal spiral, E/S0, and irregular galaxies ($\gtrsim 70\%$). Clearly interacting galaxies account for $\lesssim 30\%$. Our result is based on a combination of UV and IR luminosities but is dominated by IR-luminous objects. Wolf et al. (2005) have examined the UV-luminous objects alone and also find that most of the rest-frame UV flux density at $z \sim 0.7$ is in morphologically undisturbed galaxies.

These results have important implications for the physical mechanisms that drive the factor-of-3 decline in cosmic-averaged comoving SFR density from $z \sim 0.7$ to the present day. Because clearly interacting galaxies—with morphologies suggestive of major galaxy mergers or merger remnants²¹—contribute much less than half of the $z \sim 0.7$ SFR density, the drastic decline in cosmic SFR is only *partially* driven by the decreasing frequency of major galaxy mergers at the present day (e.g., Le Fèvre et al. 2000; Patton et al. 2002). Instead, the dominant driver is a strong decrease in SFR in morphologically undisturbed spiral galaxies. It is possible that the decreasing star formation activity of spiral galaxies is driven primarily by gas supply and consumption in a purely quiescent mode of star formation. However, it is also possible that even in spiral galaxies much star formation activity is triggered by relatively minor tidal interactions, which function to trigger internal instabilities such as spiral arms or bars, enhancing their SFR. Our observations cannot sensitively test these competing hypotheses at this stage: deeper redshift surveys and exploration of their gas content through, e.g., CO mass determination from the Atacama Large Millimeter Array will start to allow us to test the relative importance of these physical processes.

6. EXPLORING THE DEMISE OF STAR FORMATION IN MASSIVE GALAXIES

We turn now to exploring the relationship between SFR and stellar mass at $z \sim 0.7$, comparing it to that at $z \sim 0$. We choose to explore the “specific SFR,” i.e., the SFR per unit stellar mass. This is closely related to the more model-dependent birthrate parameter, $b = \text{SFR}/\langle \text{SFR} \rangle$, where $\langle \text{SFR} \rangle$ is the past-averaged

²¹ It is worth noting that relatively advanced merger remnants are also classified as clear interactions, until their tidal features have dissipated. Owing to the long dynamical times at large galactic radii, we expect that major mergers are classified as clearly interacting well after the major final burst of star formation has ceased.

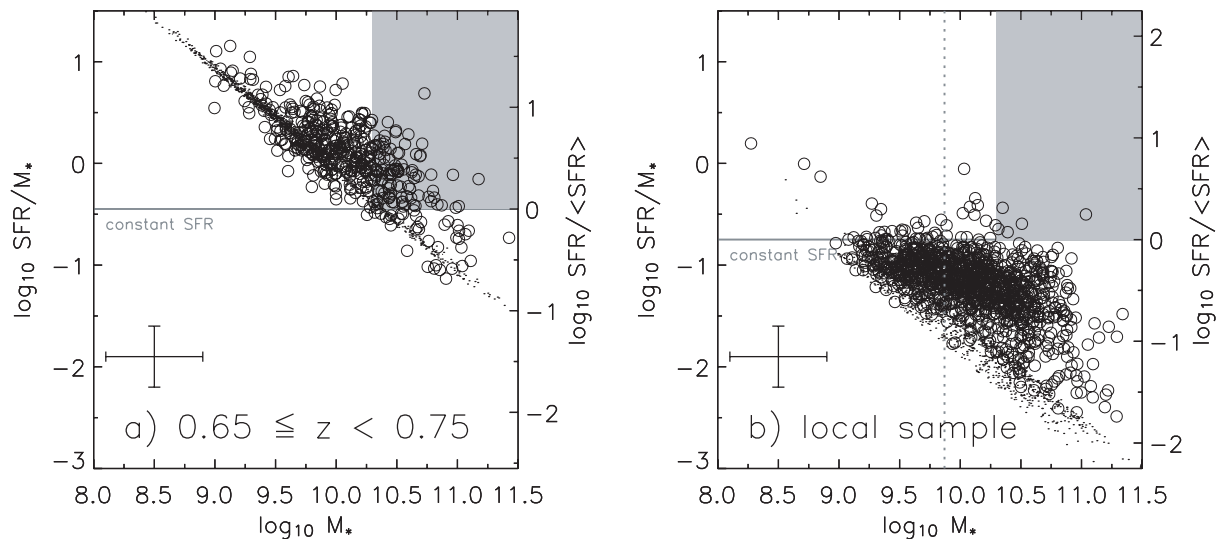


FIG. 4.—Specific SFR as a function of galaxy stellar mass, in solar units. (a) SFR per Gyr per unit stellar mass as a function of stellar mass for the $z \sim 0.7$ galaxy sample. Plotted on the right-hand axis is the birthrate parameter $b = \text{SFR}/\langle \text{SFR} \rangle$. Galaxies detected at $24 \mu\text{m}$ are shown with open circles; nondetections have upper limits shown by points. (b) SFR per Gyr per unit stellar mass as a function of stellar mass for the local comparison sample. Again, the birthrate parameter is plotted on the right-hand axis for comparison [the offset between (a) and (b) is because of the difference in the age of the universe at the two redshift intervals of interest]. IR detections are shown as open circles; nondetections are denoted by points. The dotted line shows the minimum mass for which the sample is complete. In both panels, the solid gray line shows a birthrate of unity; i.e., a constant SFR through all of cosmic history. The gray box shows the position of intermediate- and high-mass galaxies with ongoing bursts of significant star formation ($b > 1$). Both data sets sample $\sim 1.2 \times 10^5 \text{ Mpc}^3$; therefore, direct comparison of both plots is fair, remembering the influence of the detection limits.

SFR. The past-averaged SFR is estimated by dividing the stellar mass by the elapsed time since star formation began in a given galaxy (see, e.g., Kennicutt et al. 1994), adjusting for the mass lost by the stellar population as it ages. Roughly 50% of initially formed stellar mass is lost within 10^9 yr for a Kroupa (2001) IMF; therefore, $b \simeq \text{SFR}/(2M_*/t_{\text{sf}})$. In estimating t_{sf} , we simplistically assume that the epoch of first star formation is at $z_f = 4$ for all galaxies; using a present-day age of the universe of 13.5 Gyr, this corresponds to $t_{\text{sf}} \sim 12$ Gyr at $z \sim 0$ and $t_{\text{sf}} \sim 6$ Gyr at $z \sim 0.7$. Despite the extra model dependence introduced by having to assume a timescale when deriving b , birthrate has the attractive feature that it compares the observed SFR with the SFR required to build up the existing stellar mass within a Hubble time (at that epoch).

In Figure 4a, we show specific SFR as a function of stellar mass for the 1436 $0.65 \leq z < 0.75$ galaxies in our sample. Owing to the detection limit of the $24 \mu\text{m}$ observations, it is impossible to detect galaxies forming stars at anything less than a constant rate ($\text{SFR}/M_* \leq 0.4$, or equivalently $b \leq 1$) for stellar masses less than $\sim 2 \times 10^{10} M_\odot$. Yet, despite this rather stringent limitation, large numbers of galaxies have been detected at $24 \mu\text{m}$, with typical specific SFRs of $\sim 1 \text{ Gyr}^{-1}$ (i.e., if the current SFR were to continue at its present rate, the stellar mass of the galaxy would double within 2 Gyr, remembering that 50% of the mass initially in stars is returned to the gas phase by stellar winds and supernovae).

Given the existence of an important population of intensely star-forming galaxies at $z \sim 0.7$, it is instructive to explore how this compares with the properties of star-forming galaxies in the local universe. We have therefore constructed a local “control” sample of galaxies, which we show in Figure 4b. We use the NASA/IPAC Extragalactic Database (NED) to select a pseudo-volume-limited sample in the range $1500 \leq cz/\text{km s}^{-1} \leq 3000$ with 2MASS K -band magnitude cut $K < 12$, and Galactic latitude $b > 30^\circ$. This sample is complete for galaxies above $M_K < -19.6$. Where they were defined, IR fluxes were also taken from NED; total 8–1000 μm IR fluxes were estimated following

Appendix A of Bell (2003) and are accurate to $\sim 30\%$. Upper limits on IR flux were roughly estimated assuming total IR fluxes just at the *IRAS* detection limit of $\sim 3 \times 10^{-11} \text{ ergs cm}^{-2} \text{ s}^{-1}$ (the conclusions do not depend on the choice of this limiting flux). A legitimate and unavoidable concern is the inhomogeneous completeness properties of NED redshifts. For the purposes of volume estimation, we estimate an overall NED redshift completeness from the number of $K < 12$, $b > 30^\circ$ galaxies with redshifts divided by the number of $K < 12$, $b > 30^\circ$ galaxies both with and without redshifts: 14350/23658 (or 61%). Thus, the estimated total volume probed is $71,500 \times 0.61 \text{ Mpc}^3$. The total sample is 2177 galaxies, 1089 with IR detections and 1088 with only IR upper limits. In fact, because of large-scale overdensities in this volume, there are ~ 3 times more galaxies in this volume than one would expect on the basis of, e.g., the stellar mass functions or K -band luminosity functions of Cole et al. (2001) or Bell et al. (2003), taking into account all the relevant selection limits. To reflect this overdensity, we assign an “effective volume” to the sample of $\sim 1.2 \times 10^5 \text{ Mpc}^3$; this effective volume matches the actual volume in the $0.65 \leq z < 0.75$ slice. Accordingly, we use this control sample unaltered, with the rationale that in the two panels of Figure 4 we are comparing galaxies from the same effective volumes at both cosmic epochs. None of our conclusions are affected by the detailed choice of volume or, indeed, comparison sample. Different NED-derived samples can be chosen, or a sample of GEMS/MIPS galaxies with redshifts $0.1 \leq z < 0.2$ can be used as a control, with unchanged results but a reduced number of comparison galaxies.

Stellar masses and SFRs for the local comparison sample were estimated assuming a Kroupa IMF. Stellar masses were estimated directly from the K -band absolute magnitudes (where Hubble flow distances are used, for simplicity) assuming a single K -band stellar M/L of 0.6 in solar units, appropriate for a Kroupa IMF (following Bell et al. 2003; Cole et al. 2001). SFRs were estimated from total IR flux following equation (4) of Bell (2003) adjusted to a Kroupa IMF and are not corrected for any (typically modest; $\leq 30\%$) contribution to the dust heating from

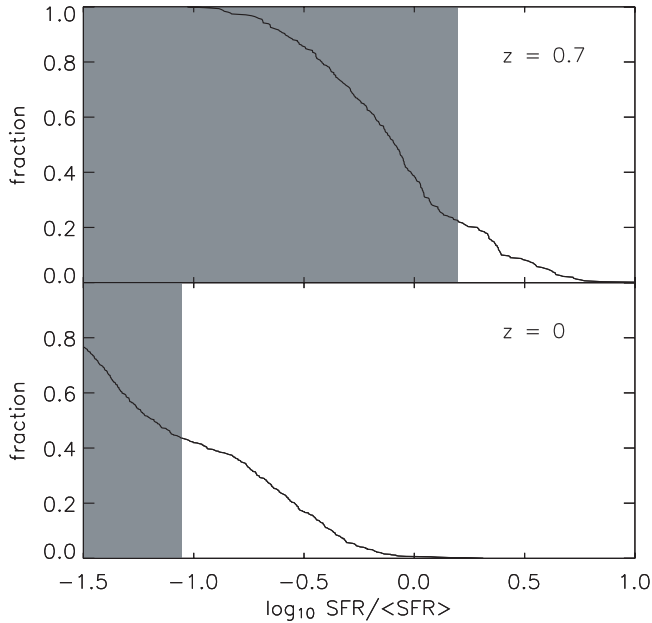


FIG. 5.—Cumulative distribution of the birthrates of massive galaxies with $M_* > 2 \times 10^{10} M_\odot$. The gray shaded region denotes the area over which upper limits on birthrates contribute to the distribution (i.e., the shape of the cumulative distribution in the gray shaded area is strongly biased toward high birthrates).

old stellar populations (like the SFR estimates constructed using the $24 \mu\text{m}$ data). The stellar masses and SFR estimates are accurate to ~ 0.3 dex, assuming a universally applicable stellar IMF, and are directly comparable with stellar masses and SFRs for the $z \sim 0.7$ redshift slice.

We compare the distribution of specific SFRs and stellar masses in the $z \sim 0.7$ sample and the local control sample in Figure 4; the cumulative histogram of birthrates is given in Figure 5. Both data sets effectively sample $\sim 1.2 \times 10^5 \text{ Mpc}^3$; therefore, in the regions where both data sets are complete, it is fair to compare the relative distributions of datapoints. The local sample is characterized by a broad distribution of star-forming galaxies with specific SFRs between 0.03 and 0.2 ($0.1 \lesssim b \lesssim 1$, i.e., slowly declining SFR through cosmic history). Furthermore, where the detection limits permit, one observes a sizeable population of galaxies with very low specific SFRs $\lesssim 0.01$, indicative of a largely non-star-forming subpopulation of (primarily early type) galaxies. There are very few galaxies with bursts of star formation that are adding significantly to their existing stellar mass (i.e., birthrates $b \gtrsim 1$). In particular, at stellar masses in excess of $2 \times 10^{10} M_\odot$, where the sample is essentially complete, five of 699 ($< 1\%$) galaxies have $b \geq 1$ (Fig. 4, *gray shaded region*).²² While there are significant systematic uncertainties in both SFR and stellar mass, it is impossible to accommodate a large population of starbursting intermediate- and high-mass galaxies in the local universe. This result is insensitive to the adoption of a variety of plausible prescriptions for SFR and stellar masses, and indeed the rarity of galaxies with $b \geq 1$ at $M_* > 2 \times 10^{10} M_\odot$ is apparent from Figure 24 of Brinchmann et al. (2004), who analyze accurate emission-line-derived SFRs from the Sloan Digital Sky Survey.

In stark contrast, turning to the $z \sim 0.7$ sample, there are a large number of massive galaxies with intense star formation.

Quantitatively, at stellar masses in excess of $2 \times 10^{10} M_\odot$, 120 of 311 (39%) of galaxies are forming stars at a rate faster than their past-averaged rate ($b \geq 1$; Fig. 4, *gray shaded region*).²³ While there are always significant systematic uncertainties, including estimation of total IR luminosity, SFRs, and stellar masses, these differences are large enough to be robust to systematic uncertainties of greater than a factor of 3.²⁴ In addition, where possible we have minimized the opportunities for systematic error by using IR-derived SFRs in both cases, and equivalent SFR and stellar mass calibrations. Indeed, adoption of the $0.1 \leq z < 0.2$ GEMS/MIPS sample as the “local” control sample yields only one galaxy with $b \geq 1$ out of 41 galaxies with $M_* \geq 2 \times 10^{10} M_\odot$. In this case, identical methodologies have been used for the $0.1 \leq z < 0.2$ and $0.65 \leq z < 0.75$ samples.

Recalling the conclusions reached in § 5, it is worth briefly commenting on the visual morphologies of galaxies with $M_* \geq 2 \times 10^{10} M_\odot$. Seventy of 124 massive spiral (Sa–Sd) galaxies, four of five massive irregular galaxies, and 18 of 23 Pec/Int galaxies have $b \geq 1$, i.e., are undergoing significant bursts of star formation. In contrast, only 20 of 138 massive E/S0 galaxies are forming stars intensely.²⁵ Therefore, roughly $\frac{1}{2}$ of spiral, irregular, and clearly interacting galaxies are undergoing starbursts at $z \sim 0.7$. Furthermore, the starbursting population is dominated by spiral galaxies rather than Pec/Int galaxies. This reinforces the conclusions of § 5; even among the most intensely star-forming $z \sim 0.7$ galaxies, the vast majority are not forming stars intensely because of a recent major merger.

Taken together, it is fair to conclude that while a large fraction of intermediate- and high-mass galaxies were forming stars intensely 7 Gyr ago, almost none are at the present epoch. Furthermore, these intensely star-forming galaxies are primarily morphologically undisturbed, indicating that major mergers are not responsible for the bulk of this intense star formation. Instead, physical properties that do not strongly affect galaxy morphology—for example, a larger abundance of gas at earlier times or weak interactions with small satellite galaxies—appear to be responsible for the high SFRs.

7. DISCUSSION

7.1. Comparison with Previous Results

Our results confirm and extend the previously observed rapid evolution in the number of IR-luminous galaxies at intermediate and high redshift (e.g., Elbaz et al. 1999; Chary & Elbaz 2001; Papovich et al. 2004) and with the drastic decline in the space density of intensely star-forming galaxies as probed with a variety of different SFR indicators (e.g., Cowie et al. 1996; Wolf et al. 2003; Bauer et al. 2005). Furthermore, we have been able to estimate the stellar masses of these intensely star-forming systems, finding that almost all of the intensely star-forming galaxies with $L_{\text{IR}} \gtrsim 10^{11} L_\odot$ (luminous infrared galaxies [LIRGs]) seen at intermediate redshift have stellar masses in excess of $\sim 10^{10} M_\odot$

²³ If starbursts were defined by high specific SFRs instead, the difference between $z \sim 0.7$ and the present day would be even more striking.

²⁴ It is likely that our neglect of heating of dust by old stellar populations affects galaxies with low b -values preferentially, artificially inflating their estimates of SFR and therefore b . From inspection of Fig. 4 this is likely to affect the most massive galaxies the most severely and will affect the low-redshift sample more acutely than the $z \sim 0.7$ sample. Thus, if the heating of dust by old stars were accounted for by detailed SED modeling, it is likely that the conclusions would remain unchanged or further strengthened.

²⁵ The total is 290 galaxies, which is lower than the COMBO-17+MIPS number of 311 galaxies owing to the smaller areal coverage of GEMS.

²² Galaxies with $M_* > 2 \times 10^{10} M_\odot$ contain roughly 70% of present-day stellar mass (Bell et al. 2003).

(Fig. 4). This is in agreement with, e.g., Franceschini et al. (2003) and Zheng et al. (2004), who used optical and NIR data to estimate the stellar masses of ISOCAM $15\ \mu\text{m}$ -selected LIRGs, finding stellar masses in excess of $\gtrsim 10^{10} M_{\odot}$, and Le Floch et al. (2004), who explore the properties of 26 $1 \lesssim z \lesssim 2.5$ IR-luminous sources with *Spitzer*, finding significant stellar masses for their sample of LIRGs.

Our conclusion that a decline in major interaction rate is not the primary cause of the decline in cosmic SFR since $z \sim 0.7$ also confirms and extends previous observations. Follow-up observations of fields targeted by *ISO* tentatively suggested that the rapidly evolving IR-luminous population may not be composed exclusively of strongly interacting galaxies. Flores et al. (1999) found that only six of 16 galaxies in a sample with *ISO* and *HST* data had strongly disturbed morphologies, while the rest were disk-dominated, E/S0, or unresolved. Zheng et al. (2004) extended their work to a sample of 36 *ISO*-selected LIRGs at $z \leq 1.2$, finding that 17% of their sample were obvious mergers and placing an upper limit of 58% on the merger fraction. Our study places these indications on firm ground, pushing to fainter limits of $\sim 6 \times 10^{10} L_{\odot}$ with an order of magnitude larger sample of galaxies.

7.2. How Much Dust Can Be Heated by AGNs at $z \sim 0.7$?

It is worth discussing the contribution of AGNs to the $24\ \mu\text{m}$ total luminosity density. To aid in identifying AGNs, we use the *Chandra* data for the CDFS to select AGN candidates. The *Chandra* footprint on the CDFS (Alexander et al. 2003) is considerably smaller than the GEMS and MIPS coverage of the field; therefore, in this section we consider only galaxies falling completely within the *Chandra* coverage. This area contains 3122 galaxies with COMBO-17 photometric redshifts; the small subsample classified by COMBO-17 as galaxies with $0.65 \leq z < 0.75$ and detected by *Chandra* comprises 22 galaxies; 0.5–8 keV source fluxes and errors are taken from Alexander et al. (2003).

While highly luminous X-ray sources are invariably AGNs, at fainter limits a contribution from star-forming galaxies is expected. To test this possibility, we compare $24\ \mu\text{m}$ -derived IR luminosities and X-ray luminosities for these 22 $z \sim 0.7$ galaxies in Figure 6. The shaded area shows the expected locus of star-forming galaxies, derived from the empirical relationship between X-ray and k -corrected 1.4 GHz radio luminosities (Fig. 1 of Cohen 2003) coupled with the radio SFR calibration of Bell et al. (2003), accounting for the 0.3 dex empirical scatter in the correlation.²⁶ It is clear that only one galaxy has X-ray emission that is consistent with a star formation origin; the others have excess X-ray emission indicative of an AGN contribution.

Considering the 21 AGN-dominated X-ray sources, we find a total IR luminosity between 3.4×10^{12} and $4 \times 10^{12} L_{\odot}$, where in the first instance we ignore upper limits and in the second instance we take upper limits to represent marginal detections. The total IR luminosity in *all* detected sources in the *Chandra* footprint is $2.6 \times 10^{13} L_{\odot}$, increasing to $5.4 \times 10^{13} L_{\odot}$ if all non-detections are taken as marginal detections at the $83\ \mu\text{Jy}$ limit. Accordingly, we estimate that $\lesssim 15\%$ of the total IR $0.65 \leq z < 0.75$ luminosity density is in sources with significant AGN emission. Clearly, the contribution to the IR luminosity density

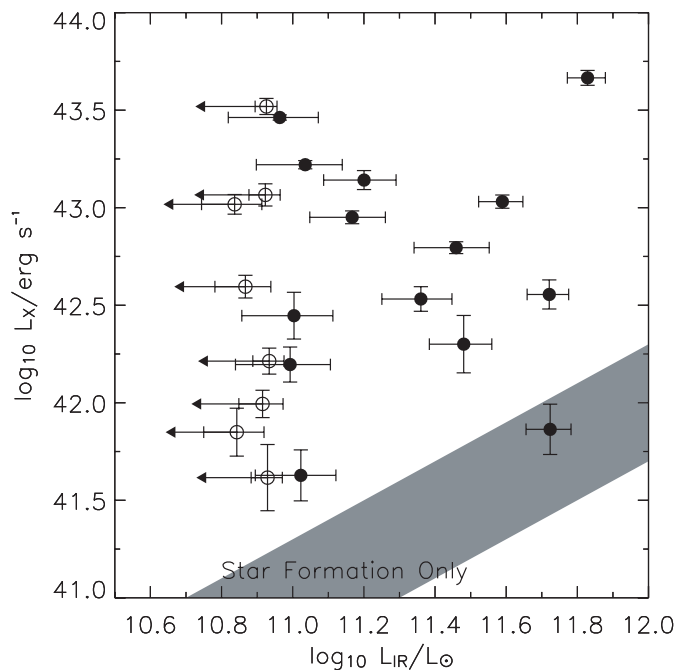


FIG. 6.— Comparison of 0.5–8 keV observed-frame *Chandra* X-ray luminosities with $24\ \mu\text{m}$ -derived total IR luminosities for the 22 $0.65 \leq z < 0.75$ *Chandra*-selected galaxies with optical detections. Filled circles denote MIPS detections, whereas open circles with limits denote MIPS upper limits only. The IR luminosity errors include uncertainty in conversion to total IR. The shaded area shows the expected locus of star-forming galaxies.

of AGN-heated dust may be substantially lower, as the IR luminosity in these galaxies may come from star formation. On the other hand, we have not accounted for any contribution of AGNs to the IR luminosities of galaxies not detected by *Chandra*; bearing in mind that the *Chandra* observations reach deep enough to start probing star formation-powered X-rays from galaxies with $L_{\text{IR}} \sim 10^{11} L_{\odot}$, one hopes that the AGNs in non-AGN-dominated galaxies will be weak and will contribute relatively little to the total IR. This conclusion is consistent with recent *ISO* and *Spitzer* results, finding 10%–20% contributions at 15 and $24\ \mu\text{m}$, respectively (Fadda et al. 2002; Franceschini et al. 2005), and with Silva et al. (2004), who model the AGN contribution to the IR background, suggesting that 10%–20% of the IR background at mid-IR wavelengths is from AGNs and their host galaxies (the AGNs alone account for 5% of the IR background in this model).

7.3. Comparison with Theoretical Expectations

Gasdynamical processes, such as star formation or feedback, are currently very challenging to include in models of galaxy formation and evolution, owing largely to important resolution limitations. As a result of the complexity of these processes, it has been impossible to converge on a robust description of star formation; instead, a wide range of empirically motivated prescriptions on kiloparsec or larger scales have been adopted (e.g., Somerville & Primack 1999; Springel & Hernquist 2003a; Barnes 2004). Current models tend to reproduce the cosmic SFH reasonably well (e.g., Cole et al. 2000; Somerville et al. 2001; Springel & Hernquist 2003b). A few models have started to incorporate detailed dust prescriptions and can model the evolution of IR-bright galaxies (e.g., Granato et al. 2000; Balland et al. 2003). While the progress is very encouraging, detailed observations such as the $24\ \mu\text{m}$ number counts are rather poorly reproduced by the models (Papovich et al. 2004), reflecting the

²⁶ This locus does not account for the mild X-ray k -corrections in the observed frame 0.5–8 keV X-ray luminosity but was defined for galaxies with $0.4 \leq z \leq 1.3$ with a median redshift of 0.76 and so will be accurate to ~ 0.1 dex (Cohen 2003). It is worth noting that the use of the SFR calibration of Cohen (2003) results in a similar locus to within 0.1 dex.

difficulty of the “gastrophysics” that must be tackled to properly reproduce the full richness of the observational data sets. For this reason, we focus in this section on qualitative features of the models, rather than a detailed comparison of IR luminosity functions, or the distribution of stellar masses and morphologies as a function of IR luminosity.

Somerville et al. (2001) present a “collisional starburst” model, in which major (with mass ratios $<4:1$) and minor (with mass ratios between $4:1$ and $10:1$) mergers trigger an episode of rapid star formation, with a star formation efficiency that increases toward lower mass ratio (i.e., is higher for major mergers). At $z \sim 0$, Somerville et al. (2001) predict that 35% of star formation is triggered by minor mergers and 2.5% of star formation is triggered by major mergers. At $z \sim 0.7$, 50% of star formation is triggered by minor mergers and 3.5% by major mergers. Thus, they predicted that the steep drop in the cosmic SFR since $z \sim 1$ is not caused by changes in the major merger rate; however, in their model a significant part of the drop reflects a declining rate of minor mergers. There are a number of important uncertainties: a lowered star formation efficiency in minor interactions would shift more star formation into major mergers because more gas would be available to form stars in major mergers, tidal interactions (e.g., flybys) are not included in the model, untriggered star formation in a galaxy with triggered star formation is not included in the census of triggered star formation, and our observational census of “clearly interacting” galaxies may well include a significant fraction of minor mergers and tidal interactions.

Nonetheless, it is encouraging that the observations and at least this model are reasonably consistent in the sense that major galaxy mergers do not drive the declining cosmic SFR from $z \sim 1$ to the present day. At present, models cannot clearly predict which processes dominate: while minor mergers and tidal interactions may dominate (Somerville et al. 2001), it is also possible that a dwindling gas supply could dominate (Cole et al. 2000; Somerville et al. 2001), depending on the efficiency of triggered star formation in the real universe.

7.4. Improvements

There are a number of areas that need to be improved to more fully understand these results and to illuminate the physics driving the cosmic SFH. We mention a few specific examples here. A more complete, ground-based and IRAC near-IR–selected photometric and/or spectroscopic sample covering comparable or larger areas will be required to push our understanding past $z \sim 1$, into the regime where we observe rapid cosmic star formation. A wide range of morphological disturbance diagnostics must be developed and robustly tested (see, e.g., Conselice et al. 2003; Lotz et al. 2004 for some promising examples of this kind of technique). Total L_{IR} and SFR calibrations must be tested thoroughly using IR spectral data coupled with 70 and 160 μm imaging data where available. This must be accompanied by a fuller analysis of local, well-studied control samples to explore the fraction of L_{IR} coming from dust heated by optical light from old stellar populations, and possible metallicity dependences in IR SEDs. The IR properties of high-redshift AGNs must be better constrained, including constraints on the fraction of light emitted by AGN-heated dust compared with dust heated by associated star formation in the AGN host. Yet, the two main conclusions of this paper—the rapid demise of intermediate- and high-mass star-forming galaxies between $z \sim 0.7$ and the present day, and the limited importance of major mergers in driving the declining cosmic SFR—are likely to hold even after these studies are completed.

8. CONCLUSIONS

In this paper, we have explored the 24 μm –derived IR properties of an optically selected sample of 1436 galaxies with $0.65 \leq z < 0.75$ in the CDFS. Optical IDs, photometric redshifts, and morphologies were obtained from the COMBO-17 and GEMS surveys. From examination of local LIRGs and ULIRGs and exploration of COMBO-17’s photometric redshift accuracy as a function of IR luminosity, we argue that the optical selection should not introduce any special bias against intensely star-forming obscured galaxies. Under the assumption that the mid-IR properties of $z \sim 0.7$ galaxies are spanned by calibrating samples in the local universe, we have derived total IR luminosities for the 442 galaxies detected at better than 5σ at 24 μm . We used these data, in conjunction with the optical data, to estimate SFRs and stellar masses.

We have found the following:

1. Galaxies with X-ray–luminous AGNs contribute $\leq 15\%$ toward the integrated $z \sim 0.7$ IR luminosity density.
2. The IR-to-UV ratio is a strong, increasing function of total SFR; this relation shows a ≥ 0.5 dex scatter. There is no evidence for evolution of this relationship over the last 7 Gyr.
3. Morphologically normal galaxies show a strong relationship between their optical and IR properties. Optically blue early-type and spiral galaxies are IR-bright. Optically red early-type galaxies and a significant fraction of red spiral galaxies are not detected at 24 μm . Most galaxies on the red sequence are genuinely old, red, and dead.
4. Dust strongly shapes the optical properties of morphologically peculiar galaxies. The majority of obviously interacting galaxies are detected at the star formation–sensitive 24 μm band, despite showing the full range of optical colors from very blue through to very red.
5. Clearly interacting galaxies with morphologies suggestive of major galaxy mergers contribute at most 30% of the integrated IR luminosity density at $z \sim 0.7$. Bearing in mind that there is a factor of 3 reduction in cosmic IR luminosity density between $z \sim 0.7$ and the present day, this suggests that a declining major merger rate can only form a small part of this drop in cosmic SFR.
6. Morphologically normal galaxies (spirals, ellipticals, and Magellanic irregulars) form more than 70% of the integrated IR luminosity density in the $z \sim 0.7$ slice. This implies that physical processes that do not strongly affect galaxy morphology, such as gas consumption and weak tidal interactions with small satellite galaxies, are likely responsible for the drastic decline in cosmic SFR since $z \sim 0.7$.
7. At $z \sim 0.7$, nearly 40% of intermediate- and high-mass galaxies are actively starbursting (i.e., they have $M_* \geq 2 \times 10^{10} M_\odot$ and $b \geq 1$). In contrast, only 1% of $z \sim 0$ galaxies with $M_* \geq 2 \times 10^{10} M_\odot$ are undergoing such active star formation. The declining SFR since $z \sim 0.7$ is driven by drastic evolution in the SFRs of intermediate- and high-mass galaxies, rather than starbursting dwarf galaxies.

This work is based (in part) on observations made with the *Spitzer Observatory*, which is operated by the Jet Propulsion Laboratory, California Institute of Technology, under NASA contract 107. Support for this work was provided by NASA through contract 960785 issued by JPL/Caltech. Support for the GEMS project was provided by NASA through grant GO-9500 from the Space Telescope Science Institute, which is operated by the Association of Universities for Research in Astronomy,

Inc., for NASA, under contract NAS5-26555. E. F. B. was supported by the European Community's Human Potential Program under contract HPRN-CT-2002-00316, SISCO. C. W. was supported by a PPARC Advanced Fellowship. D. H. M. acknowledges support from NASA under LTSA grant NAG5-13102 issued through the Office of Space Science. This publication made use of NASA's Astrophysics Data System Bibliographic Services. This research has made use of the NASA/IPAC Extra-

galactic Database (NED), which is operated by the Jet Propulsion Laboratory, California Institute of Technology, under contract with the National Aeronautics and Space Administration. This publication makes use of data products from the Two Micron All Sky Survey, which is a joint project of the University of Massachusetts and the Infrared Processing and Analysis Center/California Institute of Technology, funded by NASA and the National Science Foundation.

APPENDIX A

ARE MOST STARBURSTS IN THE COMBO-17 SAMPLE?

A possible source of bias could be that the most heavily obscured $z \sim 0.7$ star-forming galaxies may be too optically faint to be reliably picked up and/or correctly classified by COMBO-17. Indeed, there are many MIPS sources without photometric redshifts ($m_R \gtrsim 24$) or even detections ($m_R \gtrsim 25.5$) from COMBO-17. Without a comprehensive multiwavelength photometric redshift analysis we cannot definitively address this issue. Yet, we explore this issue briefly here to assess the potential scale of the biases, choosing to focus on two key issues: optical detectability and redshift accuracy.

One key point is that of optical brightness. In terms of affecting the total IR luminosity density or skewing the fractions of IR luminosity from each morphological type, the most IR-luminous galaxies are the most relevant; i.e., luminous ($10^{12} L_\odot > L > 10^{11} L_\odot$; LIRGs) and ultraluminous ($>10^{12} L_\odot$; ULIRGs) infrared galaxies. Thus, it is important to check whether local ULIRGs and LIRGs would be visible if placed at $z \sim 0.7$. We compare the optical properties of a sample of local universe ULIRGs and LIRGs from Surace et al. (2000) and Arribas et al. (2004) with the sample of Pec/Int galaxies from the $z \sim 0.7$ slice (Fig. 7). Photometry for these galaxies was presented in B and I bands; we corrected these for galactic foreground extinction, and transformed them to U and V absolute magnitudes using the PEGASE stellar population model (if instead one assumed a very young underlying stellar population and postulated that redder colors were due to dust alone, the transformation from $B - I$ to $U - V$ would remain unchanged at $\lesssim 0.1$ mag, owing to the strength of the age/metallicity/dust degeneracy in the optical wavelength region). In spite of their high obscurations, local ULIRGs and LIRGs are reasonably bright in the optical and, in common with $z \sim 0.7$ Pec/Int galaxies, show a wide range in galaxy colors (primarily because of the dust obscuration). Highly obscured IR-luminous galaxies are *not* faint in the optical; they are rather fainter than they would be in the absence of dust, but they are still reasonably bright and are certainly bright enough to be easily picked up at $z \sim 0.7$ to an m_R -band limit of 24.²⁷

Yet, it is not clear that these dusty galaxies will be well classified by COMBO-17's photometric redshift classifier. COMBO-17 adopts a two-dimensional stellar population and SMC extinction curve dust reddening grid for classification, allowing it in principle to classify galaxies with a wide diversity of stellar population properties and dust contents. In Figure 8 we test the performance of COMBO-17's classifier directly using redshifts from the VIMOS VLT Deep Survey (VVDS; Le Fèvre et al. 2004) as a function of the

²⁷ ULIRGs and LIRGs at $z \gtrsim 1$ will have $m_R \gtrsim 24$; therefore, optically selected redshift surveys to this limit will be unable to construct unbiased samples of IR-luminous galaxies.

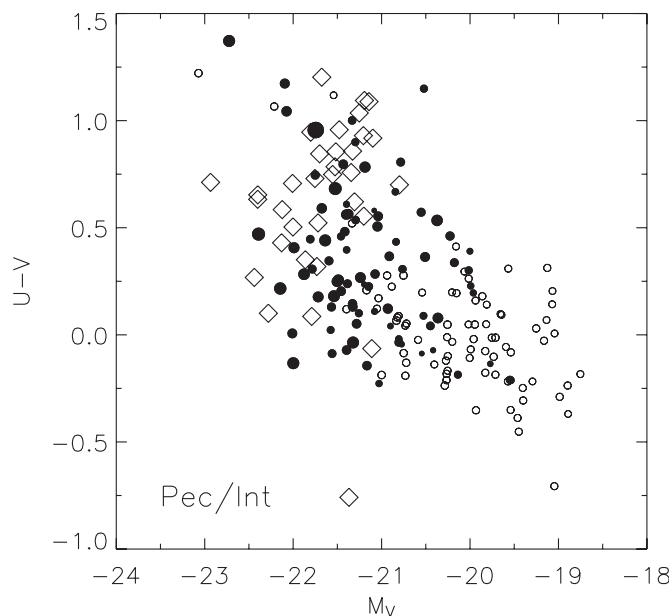


FIG. 7.—Rest-frame $U - V$ colors as a function of absolute magnitude in V band for a sample of ULIRGs and LIRGs in the local universe (*open diamonds*). Also plotted are visually classified peculiar and interacting galaxies from the $z \sim 0.7$ slice, reproduced from Fig. 2.

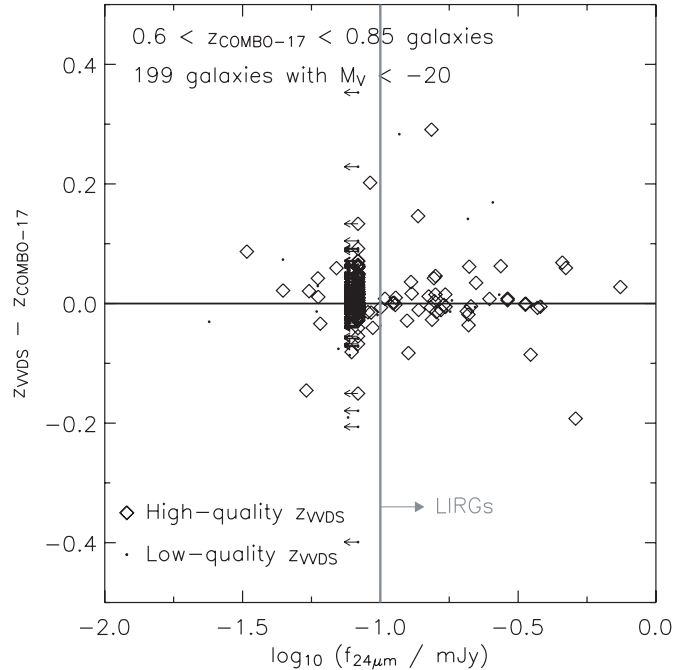


FIG. 8.— Comparison of VVDS spectroscopic and COMBO-17 photometric redshifts as a function of $24\ \mu\text{m}$ flux. Diamonds denote high-quality spectroscopic redshifts, and points denote those with more uncertain line identifications. 199 galaxies with $M_V < -20$ and $0.6 < z < 0.85$ are shown. The gray vertical line approximately shows the canonical $10^{11}\ L_\odot$ limit for LIRGs, showing a considerable LIRG population in this field and redshift range. Arrows denote $24\ \mu\text{m}$ upper limits.

$24\ \mu\text{m}$ flux. To ensure a large sample, we expand the redshift range to $0.6 < z_{\text{phot}} < 0.85$, and we require that $M_V < -20$, as this range contains the vast majority of all MIPS detections. There are a total of 199 galaxies with VVDS redshifts with estimated photometric redshifts and rest-frame V -band magnitudes in this range. Diamonds show galaxies with well-measured spectroscopic redshifts (quality flags 3/4/23/24), whereas lower quality spectroscopic redshifts, typically with less certain line identifications, are shown as points (quality flags 1/2/9/21/22). It is clear that most galaxies have well-constrained photometric redshifts; the robust σ of the distribution is $\sigma_{\text{robust}}(\Delta z) = 0.04$, independent of IR luminosity. Furthermore, the fraction of LIRGs with $\Delta z > 0.2$ is 5 of 57, or 9%, whereas the fraction of galaxies with $L < 10^{11}\ L_\odot$ with $\Delta z > 0.2$ is 7 of 142, or 5%.²⁸ The rms and outlier fraction do not strongly depend on IR luminosity.

Thus, bearing in mind that $z \sim 0.7$ IR-luminous galaxies are reasonably bright in the optical and that COMBO-17's classifier appears to work equally well for IR-bright and IR-faint galaxies, we tentatively conclude that the philosophy used in this paper—exploring the IR properties of an optically selected sample in a thin redshift slice—should not lead to any serious biases against IR-luminous, heavily obscured galaxies.

APPENDIX B

A COMPARISON OF GOODS AND GEMS MORPHOLOGIES OF IR-BRIGHT GALAXIES

An unavoidable source of error comes from classification uncertainties. With the classifications based on the one-orbit rest-frame V -band data from GEMS, $\geq 70\%$ of the SFR is in undisturbed galaxies. Yet, when one probes to fainter surface brightness levels, one will be able to better recognize tidal tails, leading to an increased fraction of interacting galaxies. To estimate the importance of this source of uncertainty, we classified a subset of 290 $0.65 \leq z < 0.75$ galaxies with deeper F850LP data from GOODS (Giavalisco et al. 2004; the GOODS southern data set forms the central $\sim \frac{1}{4}$ of the GEMS area, giving F850LP data with 5 times longer exposure time). Overall, around twice as many galaxies appeared to be clearly interacting in the deeper data set; the detailed increase in fraction varied from classifier to classifier. Almost all of the newly recognized interactions were relatively faint—GEMS-depth data are insufficient to unambiguously discern the faint tidal features that are visible in the deeper GOODS data. This issue is discussed at length in Wolf et al. (2005).

Owing to small number statistics, it is impractical to simply analyze the properties of the GOODS sample alone. We therefore derive a correction to the IR luminosity function that is tuned to reproduce the systematic difference between the GOODS and GEMS classifications for the 290-galaxy subsample covered by GOODS. For each galaxy, the nearest 25 galaxies in terms of IR luminosity are selected. Then the relative split of spiral : E/S0 : Irr : Pec/Int for these 25 galaxies using the GEMS classifications is derived and is compared with the type split derived using the GOODS classifications. This process is repeated for all galaxies, eventually building up the split of galaxy types as a function of IR luminosity in GEMS and GOODS. The difference between these type splits, as a function

²⁸ The worst outliers have lower quality VVDS spectroscopic redshifts; C. Wolf (2004, private communication) finds in a more comprehensive comparison that the VVDS spectroscopic redshifts with low-confidence quality flags 1/2/9/21/22 have a $\sim 25\%$ error rate and that COMBO-17 has an overall error rate of $\sim 5\%$ or less.

of IR luminosity, is used to correct the GEMS type-dependent IR luminosity functions in Figure 3 to roughly compensate for the shallower depth of GEMS compared to GOODS. The main difference between GOODS and GEMS is that GOODS-depth data show a statistically significant increased fraction of clear interactions at $\log_{10}(L_{\text{IR}}/L_{\odot}) \sim 11$, while the fraction of irregular and spiral galaxies at these luminosities is slightly reduced to compensate. This issue will be discussed further by C. Papovich et al. (2005, in preparation).

REFERENCES

- Adelberger, K. L., & Steidel, C. C. 2000, *ApJ*, 544, 218
 Alexander, D. M., et al. 2003, *AJ*, 126, 539
 Appleton, P. N., et al. 2004, *ApJS*, 154, 147
 Armouts, S., et al. 2001, *A&A*, 379, 740
 Arribas, S., Bushouse, H., Lucas, R. A., Colina, L., & Borne, K. D. 2004, *AJ*, 127, 2522
 Aussel, H., Cesarsky, C. J., Elbaz, D., & Starck, J. L. 1999, *A&A*, 342, 313
 Balland, C., Devriendt, J. E. G., & Silk, J. 2003, *MNRAS*, 343, 107
 Barnes, J. E. 2004, *MNRAS*, 350, 798
 Barton, E. J., Geller, M. J., & Kenyon, S. J. 2000, *ApJ*, 530, 660
 Bauer, A. E., Drory, N., Hill, G. J., & Feulner, G. 2005, *ApJ*, 621, L89
 Bell, E. F. 2003, *ApJ*, 586, 794
 Bell, E. F., & de Jong, R. S. 2000, *MNRAS*, 312, 497
 ———. 2001, *ApJ*, 550, 212
 Bell, E. F., McIntosh, D. H., Katz, N., & Weinberg, M. D. 2003, *ApJS*, 149, 289
 Bell, E. F., et al. 2004, *ApJ*, 600, L11
 Blain, A. W., Smail, I., Ivison, R. J., & Kneib, J. P. 1999, *MNRAS*, 302, 632
 Brinchmann, J., Charlot, S., White, S. D. M., Tremonti, C., Kauffmann, G., Heckman, T., & Brinkmann, J. 2004, *MNRAS*, 351, 1151
 Buat, V., Boselli, A., Gavazzi, G., & Confanti, C. 2002, *A&A*, 383, 801
 Chary, R., & Elbaz, D. 2001, *ApJ*, 556, 562
 Cohen, J. G. 2003, *ApJ*, 598, 288
 Cole, S., Lacey, C., Baugh, C. M., & Frenk, C. S. 2000, *MNRAS*, 319, 168
 Cole, S., et al. 2001, *MNRAS*, 326, 255
 Condon, J. J. 1992, *ARA&A*, 30, 575
 Conselice, C. J., Bershady, M. A., Dickinson, M., & Papovich, C. 2003, *AJ*, 126, 1183
 Cowie, L. L., Songaila, A., Hu, E. M., & Cohen, J. C. 1996, *AJ*, 112, 839
 Dale, D. A., Helou, G., Contursi, A., Silbermann, N. A., & Kolhatkar, S. 2001, *ApJ*, 549, 215
 Devriendt, J. E. G., Guiderdoni, B., & Sadat, R. 1999, *A&A*, 350, 381
 Dole, H., et al. 2004, *ApJS*, 154, 93
 Elbaz, D., Cesarsky, C. J., Chantal, P., Aussel, H., Franceschini, A., Fadda, D., & Chary, R. R. 2002, *A&A*, 384, 848
 Elbaz, D., Le Floc'h, E., Dole, H., & Marcellac, D. 2005, *A&A Lett.*, 434, 1
 Elbaz, D., et al. 1999, *A&A*, 351, L37
 Erb, D. K., Shapley, A. E., Steidel, C. C., Pettini, M., Adelberger, K. L., Hunt, M. P., Moorwood, A. F. M., & Cuby, J.-G. 2003, *ApJ*, 591, 101
 Fadda, D., Flores, H., Hasinger, G., Franceschini, A., Altieri, B., Cesarsky, C. J., Elbaz, D., & Ferrando, Ph. 2002, *A&A*, 383, 838
 Fioc, M., & Rocca-Volmerange, B. 1997, *A&A*, 326, 950
 Flores, H., Hammer, F., Elbaz, D., Cesarsky, C. J., Liang, Y. C., Fadda, D., & Gruel, N. 2004, *A&A*, 415, 885
 Flores, H., et al. 1999, *ApJ*, 517, 148
 Ford, H., et al. 2003, *Proc. SPIE*, 4854, 81
 Franceschini, A., et al. 2003, *A&A*, 403, 501
 ———. 2005, *AJ*, 129, 2074
 Gallego, J., Zamorano, J., Aragón-Salamanca, A., & Rego, M. 1995, *ApJ*, 455, 1L
 Giavalisco, M., et al. 2004, *ApJ*, 600, L93
 Glazebrook, K., Blake, C., Economou, F., Lilly, S., & Colless, M. 1999, *MNRAS*, 306, 843
 Gordon, K. D., Clayton, G. C., Witt, A. N., & Misselt, K. A. 2000, *ApJ*, 533, 236
 Gordon, K. D., et al. 2005, *PASP*, 117, 503
 Granato, G. L., Lacey, C. G., Silva, L., Bressan, A., Baugh, C. M., Cole, S., & Frenk, C. S. 2000, *ApJ*, 542, 710
 Haarsma, D. B., Partridge, R. B., Windhorst, R. A., & Richards, E. A. 2000, *ApJ*, 544, 641
 Helou, G., Khan, I. R., Malek, L., & Boemher, L. 1988, *ApJS*, 68, 151
 Hippelein, H., et al. 2003, *A&A*, 402, 65
 Hogg, D. W., Cohen, J. G., Blandford, R., & Pahre, M. A. 1998, *ApJ*, 504, 622
 Hopkins, A. M. 2004, *ApJ*, 615, 209
 Kauffmann, G., et al. 2003, *MNRAS*, 341, 54
 Kennicutt, R. C., Jr. 1998, *ARA&A*, 36, 189
 Kennicutt, R. C., Jr., Tamblyn, P., & Congdon, C. E. 1994, *ApJ*, 435, 22
 Kroupa, P. 2001, *MNRAS*, 322, 231
 Lagache, G., Dole, H., & Puget, J.-L. 2003, *MNRAS*, 338, 555
 Lagache, G., et al. 2004, *ApJS*, 154, 112
 Le Fèvre, O., et al. 2000, *MNRAS*, 311, 565
 ———. 2004, *A&A*, 428, 1043
 Le Floc'h, E., et al. 2004, *ApJS*, 154, 170
 ———. 2005, *ApJ*, submitted
 Lilly, S. J., Le Fèvre, O., Hammer, F., & Crampton, D. 1996, *ApJ*, 460, L1
 Lotz, J. M., Primack, J., & Madau, P. 2004, *AJ*, 128, 163
 Madau, P., Ferguson, H. C., Dickinson, M. E., Giavalisco, M., Steidel, C. C., & Fruchter, A. 1996, *MNRAS*, 283, 1388
 Madau, P., Pozzetti, L., & Dickinson, M. 1998, *ApJ*, 498, 106
 Mann, R. G., et al. 2002, *MNRAS*, 332, 549
 Misiriotis, A., Popescu, C. C., Tuffs, R., & Kyfalis, N. D. 2001, *A&A*, 372, 775
 Papovich, C., & Bell, E. F. 2002, *ApJ*, 579, L1
 Papovich, C., et al. 2004, *ApJS*, 154, 70
 Patton, D. R., et al. 2002, *ApJ*, 565, 208
 Pérez-González, P. G., Zamorano, J., Gallego, J., Aragón-Salamanca, A., & Gil de Paz, A. 2003, *ApJ*, 591, 827
 Pozzi, F., et al. 2004, *ApJ*, 609, 122
 Rieke, G. H., et al. 2004, *ApJS*, 154, 25
 Rigby, J. R., et al. 2004, *ApJS*, 154, 160
 Rix, H.-W., et al. 2004, *ApJS*, 152, 163
 Roussel, H., Sauvage, M., Vigroux, L., & Bosma, A. 2001, *A&A*, 372, 427
 Sanders, D. B., & Mirabel, I. F. 1996, *ARA&A*, 34, 749
 Schiminovich, D., et al. 2005, *ApJ*, 619, L47
 Silva, L., Maiolino, R., & Granato, G. L. 2004, *MNRAS*, 355, 973
 Somerville, R. S., Lee, K., Ferguson, H. C., Gardner, J. P., Moustakas, L. A., & Giavalisco, M. 2004, *ApJ*, 600, L171
 Somerville, R. S., & Primack, J. R. 1999, *MNRAS*, 310, 1087
 Somerville, R. S., Primack, J. R., & Faber, S. M. 2001, *MNRAS*, 320, 504
 Spergel, D. N., et al. 2003, *ApJS*, 148, 175
 Spinoglio, L., Malkan, M. A., Rush, B., Carrasco, L., & Recillas-Cruz, E. 1995, *ApJ*, 453, 616
 Springel, V., & Hernquist, L. 2003a, *MNRAS*, 339, 289
 ———. 2003b, *MNRAS*, 339, 312
 Steidel, C. C., Adelberger, K. L., Giavalisco, M., Dickinson, M., & Pettini, M. 1999, *ApJ*, 519, 1
 Surace, J. A., Sanders, D. B., & Evans, A. S. 2000, *ApJ*, 529, 170
 Tresse, L., Maddox, S. J., Le Fèvre, O., & Cuby, J.-G. 2002, *MNRAS*, 337, 369
 Wang, B., & Heckman, T. M. 1996, *ApJ*, 457, 645
 Wolf, C., Meisenheimer, K., Rix, H.-W., Borch, A., Dye, S., & Kleinheinrich, M. 2003, *A&A*, 401, 73
 Wolf, C., et al. 2004, *A&A*, 421, 913
 ———. 2005, *ApJ*, submitted (astro-ph/0408289)
 Yan, L., McCarthy, P. J., Freudling, W., Teplitz, H. I., Malmuth, E. M., Weymann, R. J., & Malkan, M. A. 1999, *ApJ*, 519, L47
 Zheng, X. Z., Hammer, F., Flores, H., Assémat, F., & Pelat, D. 2004, *A&A*, 421, 847